Experimental Determination of Lens Aberrations from the Intensity Point-Spread Function

Peter Dirksen[a], Joseph Braat[b], Augustus J.E.M. Janssen[d], Casper Juffermans[a] and Ad Leeuwestein[a]

[a]Philips Research Leuven, Belgium
[b]Delft University of Technology, The Netherlands
[d]Philips Research Laboratories, The Netherlands

ABSTRACT

In this paper we show various results of aberration retrieval using the pinhole method in conjunction with the extended Nijboer-Zernike theory. The experiments are performed on modern wafer scanners. Keyboard commanded offsets of the movable lens elements of the imaging tool have been used to introduce astigmatism, coma and spherical aberration in a controlled way. The method is designed to estimate these induced aberrations and we show the experimental results of the various types of aberrations created this way.

Keywords: Optical lithography, aberrations, phase retrieval, amplitude retrieval, point-spread function, extended Nijboer-Zernike theory

1. INTRODUCTION

In optical lithography, an exact knowledge of the point-spread function is required to calculate the image of an object. Projection lens aberrations cause the point-spread function to deviate from its ideal shape, the Airy disk. The impact of lens aberrations on the image performance of the lens is well known and described by various authors.[1–4] Several user tests, such as the in-situ interferometer[7] and resist based tests,[8–10] to measure aberrations exist. The Extended Nijboer Zernike theory (ENZ)[5,6] provides an analytical expression for the point-spread function including the effects of defocus and aberrations. Due to the analytical nature of the formulas the ENZ theory is not only useful to do computations in the forward direction, i.e. from aberrations to point-spread function, but also in the *reverse* direction, which amounts to aberration retrieval from the given measured 3-D intensity point-spread function.

The pinhole method[11] is an experimental method to determine the aberrations of a wafer stepper or scanner in the field, using the ENZ theory. The test pattern is an isolated transparent hole in a dark field binary mask. For a sufficiently small hole diameter, small compared to the system resolution, the image approximates the point-spread function of the lens, that is either recorded in resist or captured by a detector. The ENZ theory is flexible enough to allow for non-negligible sizes as well.

The pinhole method has a number of attractive features. The method is wavelength independent and a single mask can be used on several systems. Due to the absence of phase errors in the mask, the determination of spherical aberration is likely to be more accurate compared to methods that use a phase shifting mask. Our method determines all aberrations: not only the phase errors of the projection lens but also the transmission errors can be determined in a single experiment. The pinhole method is a true projection lens test in the sense that its results are independent of the illuminator. One numerical aperture setting, the maximum NA, is needed to characterise the lens. Finally, no simulator is needed to calibrate the results since these directly translate into $m\lambda$ wave front aberration.

Further author information: (Send correspondence to P.D.)
P.D. and C.J.S.: E-mail: peter.dirksen@imec.be, Philips Research Leuven, Kapeldreef 75, B-3001 Leuven, Belgium
J.B.: Optics Research Group, Department of Applied Sciences, Delft University of Technology, Lorentzweg 1, NL-2628 CJ Delft, The Netherlands
A.J.E.M.J. and A.L.: Philips Research Laboratories, WY-81 and WY-51, NL-5656 AA Eindhoven, The Netherlands

In this paper we show various results obtained on modern wafer scanners. Keyboard commanded offsets of the movable lens elements of the imaging tool have been used to introduce astigmatism, coma and spherical aberration in a controlled way. The pinhole method is designed to estimate these induced aberrations and we show the experimental results of the various types of aberrations created this way.

2. REVIEW OF THE EXTENDED NIJBOER ZERNIKE THEORY

In this section we briefly review the extended Nijboer-Zernike theory. The general pupil function $A \cdot exp(i\Phi)$ of the projection lens with a possible non-constant transmission amplitude A is expanded as a series of Zernike terms Z_n^m:

$$A \cdot exp(i\Phi) = \sum_{n,m} \beta_{nm} Z_n^m(\rho, \theta) \tag{1}$$

The β_{nm} coefficients fully describe the lens and can be viewed as a generalisation of the Zernike coefficients.

According to the ENZ theory, The complex amplitude of the point-spread function U is given by:

$$U(r, \phi, f) = 2 \sum_{n,m} i^m \beta_{nm} V_{nm}(r, f) \cos m\phi \tag{2}$$

with analytically known V_{nm}. The intensity $I(r, \phi, f)$ of the point-spread function after linearization, i.e. small aberrations are assumed, can be written as a linear combination of intensity basic functions:

$$\begin{aligned} I(r, \phi, f) \quad &\approx \quad 4\beta_{0,0}^2 |V_{00}(r, f)|^2 \\ &+ \quad \beta_{0,0} \sum_{(n,m)\neq(0,0)} Im(\beta_{nm}) \Psi_n^m(r, f) \cos m\phi \\ &+ \quad \beta_{0,0} \sum_{(n,m)\neq(0,0)} Re(\beta_{nm}) \chi_n^m(r, f) \cos m\phi \end{aligned} \tag{3}$$

with (r, ϕ) the polar coordinates in the image plane and f the defocus parameter. Note the separation of r and ϕ terms. Equation 3 consists of three parts: the first part is the aberration free term, i.e. the through focus Airy disk. The second part with intensity basic functions Ψ_n^m and coefficients $Im(\beta_{nm})$ represents the phase errors of the lens. The third part with intensity basic functions $\chi_n^m(r, f)$ and coefficients $Re(\beta_{nm})$ represent the transmission errors. We have introduced the intensity basic functions:

$$\Psi_n^m(r, f) = \gamma_m Re\{i^{m+1} V_{00}^* V_{nm}\}\ , \quad \chi_n^m(r, f) = \gamma_m Re\{i^m V_{00}^* V_{nm}\}\ . \tag{4}$$

with $\gamma_m = 4$, $m = 1, 2, \cdots$, $\gamma_0 = 8$.

The finite hole size can be taken into account by replacing f by a complex defocus parameter throughout the formula's. Now a relative large diameter may be used experimentally, significantly reducing the required exposure dose and making the experimental procedure much more practical. A detailed description and definitions of the various functions is given in the appendix.

Figure 1 shows the aberration free point-spread function, or Airy pattern, $|V_{00}|^2$. The Airy pattern is an even function of focus. Figure 2 shows a few examples of the basic functions Ψ_n^m and χ_n^m. The upper index m corresponds to the angular dependence. For example, the $m = 0$ term describe the rotational symmetrical terms, i.e. spherical aberration. The coma terms correspond to $m = 1$, astigmatism to $m = 2$ and three point to $m = 3$. Basic functions corresponding to higher order aberrations have larger values of n and tend to have a large radial and focus extend.

The basic functions corresponding to phase errors Ψ_n^m and transmission errors χ_n^m have opposite through-focus symmetry. As a consequence the phase errors and transmission errors can be separated in an aberration retrieval experiment. The symmetry properties are summarized in the table below:

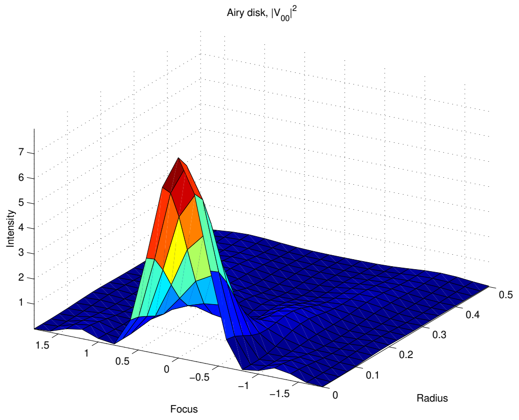

Figure 1: The Airy disk $|V_{00}(r,f)|^2$ as a function of the radius and focus.

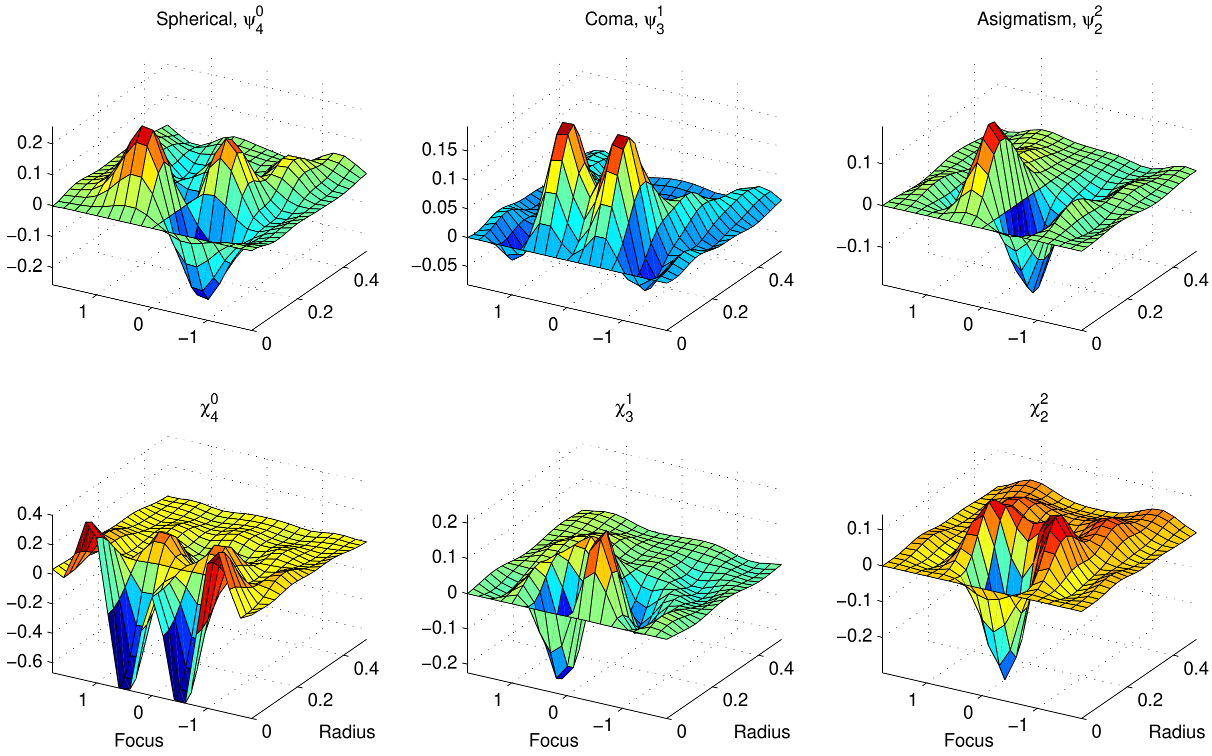

Figure 2. Examples of the intensity basic functions as a function of radius and focus: The top row shows the intensity basic functions corresponding to spherical, coma and astigmatism phase errors. The bottom row shows the corresponding transmission intensity basic functions. Note that $\Psi_n^m(r,f)$ and $\chi_n^m(r,f)$ have opposite through-focus symmetry.

Through focus symmetry properties				
	m	n	Phase terms ψ_n^m	Transmission terms χ_n^m
Airy disk	0	0	even	
Spherical	0	$,2,4,\cdots$	odd	even
Coma	1	$1,3,5,\cdots$	even	odd
Astigmatism	2	$2,4,6,\cdots$	odd	even
Three point	3	$3,5,7,\cdots$	even	odd

$\vdots$

In fig. 3 we highlight the difference brtween a phase error and a transmission error. According to Eq. 3 the pointspread function of an aberrated lens is linear combination of the aberration free pointspread function V_{00} and Ψ_n^m and χ_n^m. As an example, figure 3 shows a point-spread function with astigmatism $m = 2$. The phase error produces the well-known elliptical deformation that changes its orientation when f is replaced by $-f$. In best focus, the basic function Ψ_2^2 vanishes and the point-spread function has rotational symmetry. Similarly the transmission error produces an elliptical deformation. However, the ellipse maintains its orientation through focus and is present even in best focus.

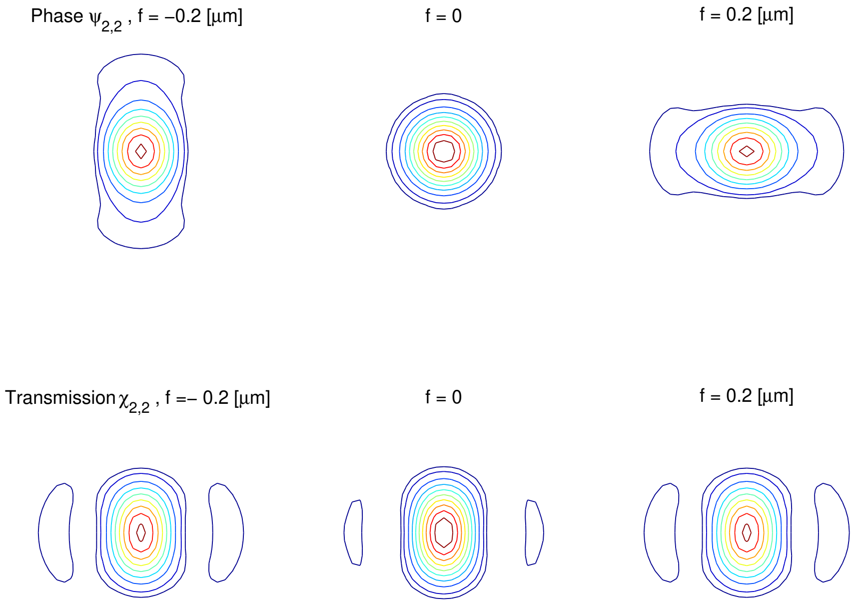

Figure 3. point-spread function at three focus values in the presence of astigmatism $m = 2$. Top row: phase error and the bottom row: transmission error.

3. EXPERIMENTAL DETERMINATION OF THE POINT-SPREAD FUNCTION

We use a simple chrome-on-quartz reticle with $4 \times 0.15 = 0.6\,\mu m$ transparent holes. The same mask can be used for different scanners, even having a different exposure wavelength: a ASML PAS5500/750 system with a $\lambda = 248$ nm, $NA = 0.70$ projection lens and a ASML PAS5500/950 system with a $\lambda = 193$ nm, $NA = 0.63$ projection lens. The reticle is imaged onto resist on a *SiON* anti-reflective coating. Using *SiON* instead of an organic anti-reflective coating has the advantage that it provides a good contrast in the SEM. First two small reference marks are exposed, using the same reticle. The coordinate system, superimposed onto the image, is shown. The relative large central image in Fig. 4, represents a single contour of the point-spread function at a certain exposure dose and defocus value. Inside this contour, the image intensity is above the resist threshold value and the resist completely develops away, leaving the *SiON* layer. Outside the contour, the SEM image shows the undeveloped resist. The procedure is repeated for a number of focus values and exposure dose settings, i.e. the reticle is exposed in a focus exposure matrix (FEM). A SEM, under job control, collects all images. The data reduction is done off-line.

Figure 5 shows a superposition of a number of contours at a single defocus value. From these we have to estimate the coefficients β_{nm} of Eq. 1 of these basic functions that represent the pupil function. The coefficients are estimated by optimising the match between the theoretical intensity and the measured intensity $I(r, \phi, f)$ patterns at several values of the defocus parameter. However, at this moment we only have resist contours as shown in fig. 5.

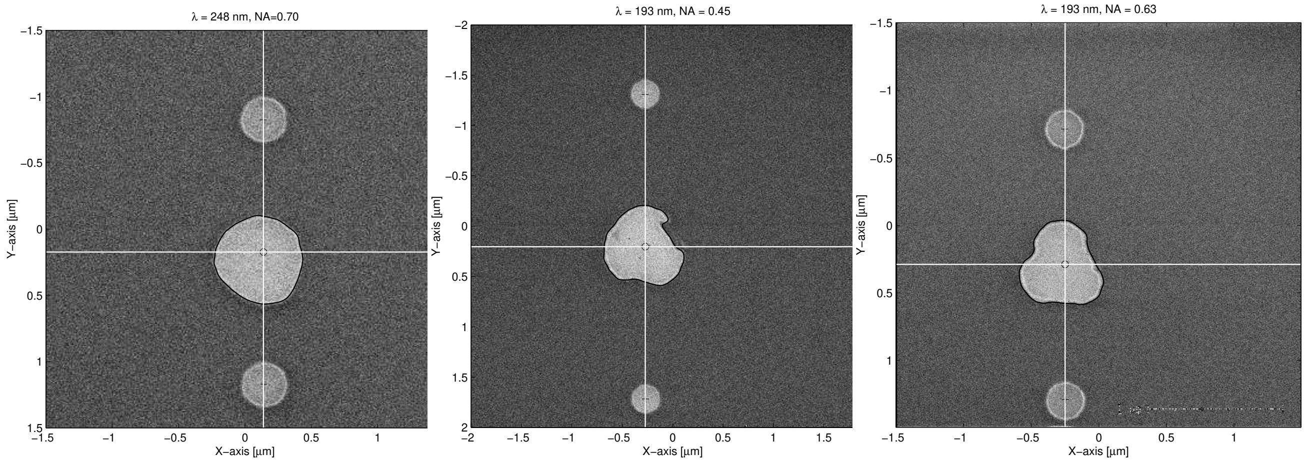

Figure 4. *This results illustrates the flexibility of the pinhole method. All experiments use the same mask and hole size. Left: Scanner PAS5500-950, $\lambda = 193$nm at a NA = 0.45 and mid NA=0.63. Right: PAS5500-700, $\lambda = 248$nm, NA =0.70.*

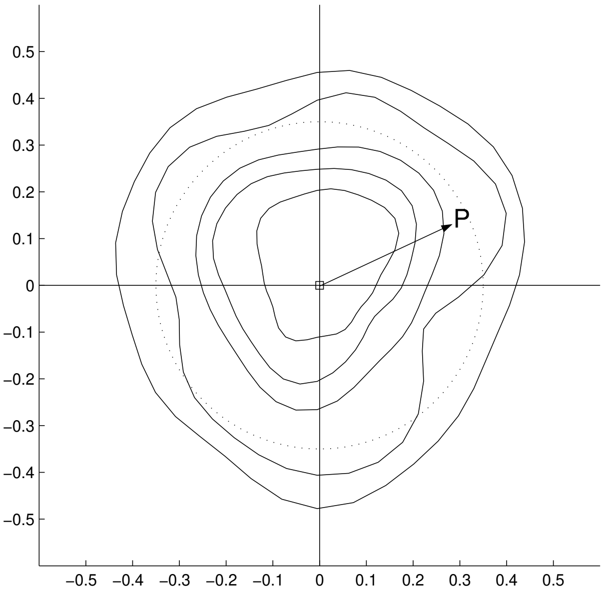

Figure 5. At one focus value a number of contours is combined into the intensity function. Scanner PAS5500-950, $\lambda = 193$nm, NA=0.63.

Effects of resist development and SEM effects are incorporated using a simple model. To convert the resist contours into the through-focus aerial image we have used a primitive model: a constant offset of 35 nm, which is an optimal value for our process, is removed from the diameter of all observed contours. An inaccuracy of this model will mainly impact the spherical transmission terms that are even through focus. But the spherical phase terms, as is indeed proven by the experiments presented above, hardly suffer from the model inaccuracy. Along the corrected contours we now know the intensity of the point-spread function.

We will solve eq. 3 for the unknown β's numerically. The way we solve eq. 3 incorporates a Fourier transform for ϕ of both sides.

$$I^m(r,f) = \frac{1}{2\pi}\int_0^{2\pi} I(r,\phi,f)\cos m\phi d\phi \tag{5}$$

To approximate the value of I in a point for a given focus value, we discrimate three cases. Inside the smallest contour we take I constant and equal to its value on that contour. Outside the contours, we take I constant and equal to its value on the greatest contour. Between two contours we will use linear interpolation to obtain values for I. We construct a path between the contours, that contains the point P. The begin and end of the path are orthogonal to the contours. Along the constructed path we suppose I linear. For the numerical integration we only consider radii smaller than the greatest radius belonging to all contours.

Figure 6 shows examples of the experimentally determined radial symmetrical part I^0. The radial symmetrical part is written as a linear combination of intensity basic functions with $m = 0$, i.e. $\Psi^{0,n}$ and $\chi^{0,n}$. Now two sets of linear equations have to be solved. The two sets of linear equations, corresponding to phase and transmission errors, decouple as $\Psi^{0,n}$ and $\chi^{0,n}$ have opposite parity with respect to their dependence on f. And thus the $\beta_{n,0}$ coefficients are estimated.

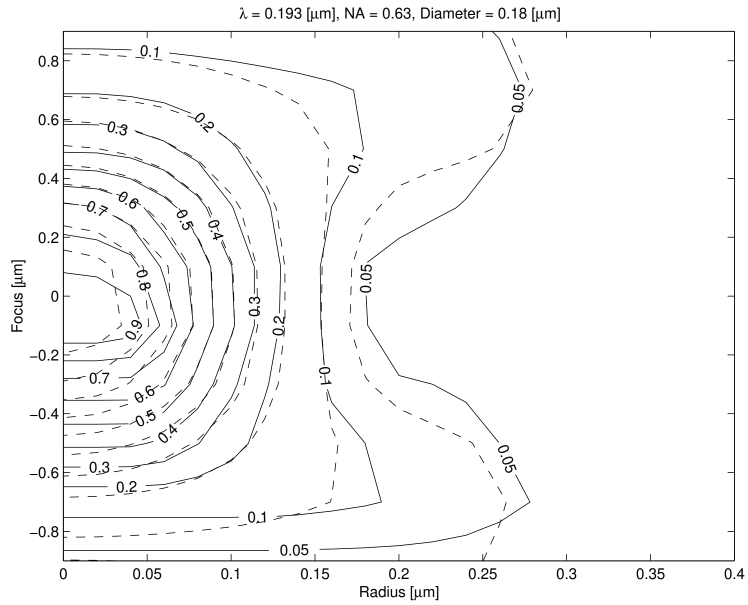

Figure 6. *The radial symmetrical part I^0 of the intensity pointspread function. Solid lines: experiment, dashed lines the retrieved intensity using the estimated $\beta_{n,0}$ coefficients. Scanner PAS5500-950, $\lambda = 193nm$, NA =0.63*

Figure 6 shows a comparison between the experimental and retrieved intensity. The goodness of fit $(mean + 3\sigma)$ is typically 8%. In a similar way the other aberrations like coma, astigmatism and three foil are estimated from the observed Fourier components I^m for $m = 1, 2, 3$ respectively.

We have compared the pinhole results with an independent aberration measurement according to the Aberration Ring Test.[9] The general picture is confirmed: the projection lens suffers from low order Y-coma, astigmatism and Y-three point and only a small amount of other aberrations such as spherical are present. There is some similarity between ART and the new pinhole method: in the ART method a phase dot is exposed to resist, that prints as a ring. In the ideal case the ring has rotational symmetry and symmetry through focus. The shape deviations, in terms of Fourier components, are a measure for the different aberration types. After calibration with a simulator, the shape deviations can be translated into aberrations. The great advantage of the new method is that its result directly translate into mwaves wavefront aberration including a split into low and high order aberrations from a single experiment. Also note that the pinhole method uses one numerical aperture setting to characterise the lens.

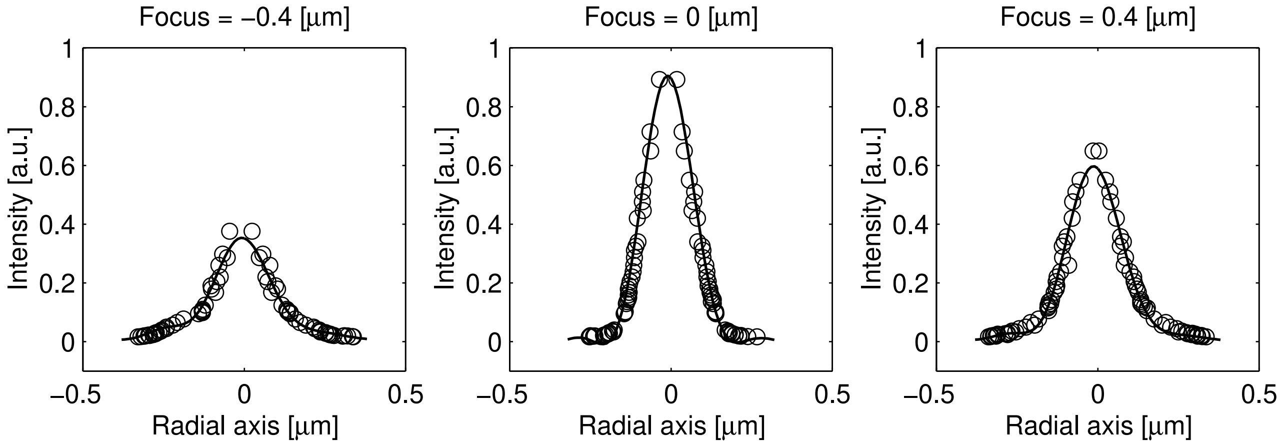

Figure 7. Through focus cross sections of the retireved intensity PSF (solid) compared to the experimental PSF (circles).

4. DETUNING EXPERIMENT

The experimental result shown in fig. 6 shows a good match between the experimental and retrieved intensity. A detuning experiment is used to validate the retrieved aberration parameters. We applied keyboard commanded offsets of the movable lens elements, reticle table height and exposure wavelength of the imaging tool to introduce aberrations in a controlled way. The pinhole method is used to estimate these induced aberrations. The experimental results are summarized in Fig. 8 where we compare the nominal state of the imaging tool to a detuned state where the aberrations have been added. The measurements are performed at a single point near the edge of the imaging field.

The first experiment is shown in Fig. 8 top. Approximately 50 mwaves of spherical has been added and this detuned state is compared to the nominal state of the tool. The experiment confirms that only spherical aberration has changed while the other aberrations remain constant. The observed aberration change is approximately equal to the amount of spherical introduced to the system.

Similar, fig. 8 mid shows the results when +50 mwaves X-coma has been added and fig. 8 bottom shows the results when +50 mwaves horizontal-vertical astigmatism has been added. At this moment we can estimate the wave front aberrations with an error typically of the order of 0.015λ.

5. SUMMARY AND DISCUSSION

In this paper we have shown various results of aberration retrieval using the pinhole method in conjunction with the extended Nijboer-Zernike theory. The detuning experiment, where commanded offsets of the movable lens elements have been used to introduce aberration, proofs that the pinhole method is able to pick up aberration changes. The pinhole method is wavelength independend as was illustrated by the experimental results obtained on a DUV and a 193 nm scanners using the same reticle. In order to estimate the aberrations, no simulator was used to 'calibrate' the results, since these directly translate into $m\lambda$ wave front aberration simply by using the aberration retrieval procedure described above.

Some improvements are possible. To convert the resist contours into the through-focus aerial image we have used a primitive resist model: a constant offset is removed from the diameter of the observed contours. An inaccuracy of the resist model will mainly impact the spherical transmission terms that are even through focus. But the spherical phase terms, as is indeed proven by the experiments presented above, hardly suffer from the

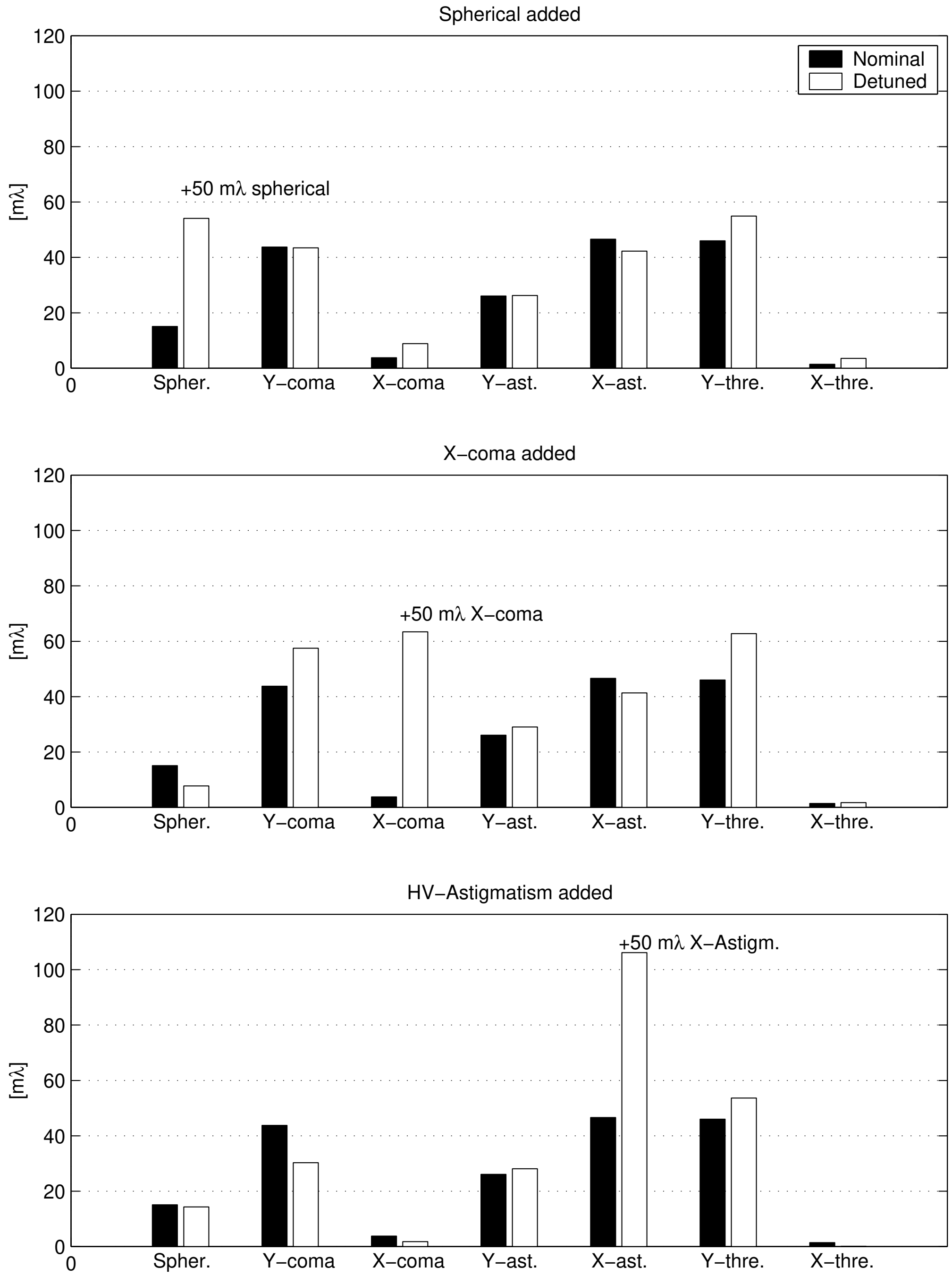

Figure 8. In the detuning experiment aberrations have been added to the imaging tool. The aberrations are retrieved and compared to the nominal state of the tool. Top: the nominal state is compared to a detuned state where +50 mwaves spherical aberration was added. Mid: nominal compared to the +50 mwaves X-coma state. Bottom: nominal compared to the +50 mwaves HV-astigmatism state.

model inaccuracy. Also we have used the linear theory of Eq. 3 to estimate the aberrations. In principle it is possible to include the quadratic terms and to make a more accurate estimate of the lens errors.

ACKNOWLEDGMENTS

The authors wish to thank Hans Kwinten, David Van Steenwinckel, Michael Benndorf and Johannes van Wingerden from Philips Reseach Leuven and Peter de Bisschop from IMEC for their valuable input and experimental support.

6. APPENDIX

Here we briefly review the mathematics to calculate the point-spread function. A detailed description, inculding a description of aberration retrieval, is given elsewhere.[5,6,11] The relationship between normalised image coordinates (x, y) and the defocus parameter f on one hand and the real space image coordinates (X, Y, Z) in the lateral and axial direction on the otherhand is given by:

$$\begin{aligned} x = X\frac{NA}{\lambda} \quad &, \quad y = Y\frac{NA}{\lambda} \\ r = \sqrt{x^2+y^2} \quad &, \quad (x,y) = (r\cos\phi, r\sin\phi) \\ f \quad &= \quad 2\frac{\pi}{\lambda}Z(1-\sqrt{1-NA^2}) \quad , \end{aligned} \tag{6}$$

with (r, ϕ) polar coordinates in the image plane. Finite hole size can be taken into account by replacing f by a complex defocus parameter $\approx f + i\pi^2/2a^2$ with a hole diameter.

For integers $n, m \geq 0$ with $n - m \geq 0$ and even, the Bessel series representation for the basic functions V_{nm} reads:

$$V_{nm}(r,f) = \exp(if)\sum_{l=1}^{\infty}(-2if)^{l-1}\sum_{j=0}^{p} v_{lj}\frac{J_{m+l+2j}(v)}{lv^l}, \ v = 2\pi r, \tag{7}$$

with v_{lj} given by

$$v_{lj} = (-1)^p(m+l+2j)\binom{m+j+l-1}{l-1}\binom{j+l-1}{l-1}\binom{l-1}{p-j}\Big/\binom{q+l+j}{l}, \tag{8}$$

where $l = 1, 2, \ldots;\ j = 0, \ldots, p$. In Eq. (8) we have set

$$p = \frac{n-m}{2} \ , \ q = \frac{n+m}{2}. \tag{9}$$

REFERENCES

1. T.A. Brunner, "Impact of lens aberrations on optical lithography." *Proceedings of the Microlithography Seminar interface*, 1996 p. 1
2. D.G. Flagello, H. van der Laan, J. van Schoot, I. Bouchoms, B. Geh, "Understanding systematic and random CD variations using predictive modelling techniques.", *Proceedings of the SPIE* **vol. 3679**, 1999 p. 162
3. C. Progler, D. Wheeler, "Optical lens specifications from the user's perspective", *Proceedings of the SPIE* **vol.3334**, 1998, p.256
4. D. G. Flagello, B. Geh, "Lithographic lens testing: analysis of measured aerial images, interferometric data and photo resist measurements." *Proceedings of the SPIE* **vol. 2726** 1996, p.788
5. A.J.E.M. Janssen, "Extended Nijboer-Zernike approach for the computation of optical point-spread functions", *JOSA A* **Vol. 19**, 2002, p. 849
6. J.J.M. Braat, P. Dirksen, A.J.E.M. Janssen, "Assessment of an extended Nijboer-Zernike approach for the computation of optical point-spread functions", *JOSA A* **Vol. 19**, 2002, p. 858

7. N.R. Farrar, A.L. Smith, D. Busath, D. Taitano, "In-situ measurement of lens aberrations", *Proceedings of the SPIE* **vol. 4000**, 2000, p. 18
8. J.P. Kirk, T.A Brunner, "Measurement of microlithography aerial image quality", *Proceedings of the SPIE* **vol.2726**, 1996, p. 410
9. P. Dirksen, C. Juffermans, R. Pellens, P. De Bisschop, "Novel aberration monitor for optical lithography", *Proceedings of the SPIE* **vol. 3679**, 1999, p. 77
10. F. Zach, C.Y. Lin, J.P Kirk, "Aberration analysis using reconstructed aerial images of isolated contacts on attenuated phase-shift masks", *Proceedings of the SPIE* **vol. 4346**, **2001** p. 1362
11. P. Dirksen, J. Braat, A.J.E.M. Janssen, C. Juffermans, Aberration retrieval using the extended Nijboer-Zernike approach, J. Microlith. Microfab., Microsyst.,**Vol.** 2, 2003, p. 61